Design and analysis of a high-performance terahertz photoconductive modulator enhanced by photonic crystal cavity

Faramarz Alihosseini
K.N.Toosi University of Technology
Zahra Heshmatpanah
K.N.Toosi University of Technology
Hesam Zandi (zandi@kntu.ac.ir)
K.N.Toosi University of Technology

Research Article

Keywords: Modulator, photonic crystal cavity, free carrier density, conductivity

Posted Date: July 5th, 2022

DOI: https://doi.org/10.21203/rs.3.rs-1770718/v1

Design and analysis of a high-performance terahertz photoconductive modulator enhanced by photonic crystal cavity

Faramarz Alihosseini[1] · Zahra Heshmatpanah[1] · Hesam Zandi[1]

[1]Department of Electrical Engineering, K. N. Toosi University of Technology, Tehran, Iran

Corresponding author: Hesam Zandi

email: zandi@kntu.ac.ir

Abstract

We propose and design a high-speed and high-performance optically controlled terahertz (THz) intensity modulator based on the free carrier modulation of a GaAs semiconductor. The device comprises a photonic crystal cavity-waveguide coupling structure for operation in the THz region. This modulator benefits from the strong interaction between the THz wave and the photoconductive substance to obtain a deep modulation with GHz speed, even with a low external optical power. The finite element method was used to calculate the most important properties of the modulator, such as the modulation depth, insertion loss, and modulation rate. The proposed modulator also demonstrated external optical power-dependent characteristics. The results indicate that the THz intensity can be modulated at a switching frequency of 1 GHz with high modulation depths of 83% and 90.3% under the continuous wave laser pumping of 50 W/cm^2 and 80 W/cm^2 respectively. In addition, this modulator exhibits efficient performance under the same pumping power with a switching frequency of up to 3 GHz. The device exhibited higher modulation depths with higher laser power intensities. The outstanding properties of the proposed structure are promising for the development of modulators and switches in THz communication systems.

Keywords Modulator · photonic crystal cavity · free carrier density · conductivity

1 Introduction

Terahertz (THz) science and technology have been widely adopted in communication systems over the past several years [1-3]. In this area, THz modulators have emerged as one of the most functional devices under intensive research and development. To efficiently modulate a THz wave, different research groups have used various techniques and materials, including metasurfaces [4-6], two-dimensional materials [7-9], liquid crystals [10, 11], nanoparticles [12], two-dimensional electron gas [13], and photonic crystals [14-16]. All this has been done to improve the modulator characteristics in terms of modulation speed, modulation depth, bandwidth, and energy efficiency. For example, Deng et al. demonstrated a modulator based on InSb gratings on the GaAs substrate with a modulation speed of 1.2 GHz and a 46.7% transmittance modulation at the frequency of 1.5 THz [17]. Another efficient THz modulator based on a composite metamaterial with double-channel heterostructure was demonstrated 1 GHz modulation speed

and 85% modulation depth [18]. Although the modulation depth up to 99.9% was achieved by modulators composed of two-dimensional materials and semiconductor heterostructures, they limit the modulation speed to the order of MHz [19-21].

THz modulators based on tuning the conductivity of a semiconductor with an external electrical signal or optical power are one of the most desirable structures which have received considerable attention [22, 23]. In this mechanism, modulating of free carrier density changes the conductivity of the substance. The amplitude of a wave passing through this substance attenuates proportionately with its conductivity. Optical modulation is preferable to electrical modulation because of its superior performance in characterizing wider bandwidth, faster speed, and higher modulation depth [24, 25]. However, for optically controlled modulators, the achievement of large modulation depths requires considerable energy consumption. As a result, it is desirable to improve the light-matter interaction by trapping the THz wave within a cavity. The better the confinement, the higher the modulation depth, but the modulation rate reduces at higher confinement. This characteristic trade-off is typical for these modulators. It is thus necessary to find an acceptable compromise between the speed of modulation and the depth.

In this study, we design an all-optical tunable THz intensity modulator based on the photoconductive properties of semi-insulating (SI) GaAs. By numerical calculation, we show that guiding the THz wave in a photonic crystal waveguide and trapping it in the cavity where the GaAs substance is, creates a strong interaction with GaAs. This introduces a high modulating effect that works with a low power optical pump. Also, show that this modulator has a high modulation rate in the order of several GHz.

2 Theory and Structure Design

The schematic of the proposed optically tunable THz modulator is shown in figure 1(a). The device comprises 2D square arrays of silicon rods. The square lattice constant and radius of rods are assumed to be a and r, respectively. As shown in figure 1(b) by making a pair of linear defects (waveguides) along the *x*-axis and removing three of the rods (cavity) along the *y*-axis which connects the two waveguides, we designed the waveguide-cavity coupling mechanism. The device is designed based on a photonic band gap to transport waves of a particular frequency along the waveguide while forbidding from going in any other direction. The cavity is beneficial to control light in a narrow frequency band or, equivalently,

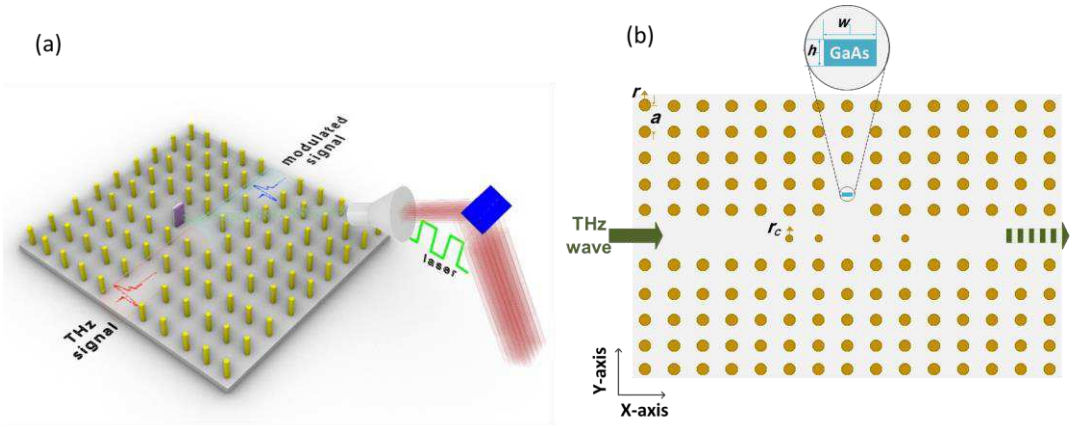

Fig. 1. Schematic of proposed THz modulator: (a) 3D view (b) top view.

trapping for a long time [26-29]. Here, we consider the two outer rods of the cavity with a radius of r_c. A THz wave having the same frequency as the cavity mode is launched into the input waveguide and coupled to the resonant cavity, and then continue to propagate into the output waveguide. Taking advantage of this condition, an SI-GaAs wafer with the thickness of h and width of w is located within the cavity.

If an optical pump with greater energy than the electronic bandgap irradiates on the GaAs, the electrons absorb photon energy and are promoted to excited states. At this point, the conductivity of GaAs which is related to its free carrier density increases. The time-dependence of the free carrier density generated within the absorption depth is given by [30]:

$$\frac{dN}{dt} = \frac{\eta_e \alpha(1-R)}{h\nu} P - \frac{N}{\tau} \quad (1)$$

where η_e is the photoconductor external quantum efficiency (we assumed that each photon generates a single electron-hole pair), α is the absorption coefficient, R is the reflectance power at the surface of GaAs, $h\nu$ is the photon energy, τ is the carrier lifetime, and P is the incident optical intensity. According to Beer-Lambert law, when an electromagnetic wave passes through a substance, its intensity attenuates exponentially as a function of distance from the surface of the material via $P(d) = P_0 \exp(-\alpha d)$. Therefore, the carrier density varies with the illumination time and depth of the substance. To calculate the spatially varying free carrier density, the GaAs layer is divided into 50 nm-thick sublayers with an approximately constant power for each sublayer. The optical parameters of GaAs are given in table 1. Manipulating the free carrier density of GaAs via the optical pumping results in a variation of GaAs permittivity and its conductivity. The permittivity of the GaAs at THz frequencies is calculated by the classic Drude model through the following expression [31, 32].

$$\varepsilon(\omega) = \varepsilon_\infty \left(1 - \frac{\omega_p^2}{\omega^2 + i\omega\gamma}\right) \quad (2)$$

Here ε_∞ is the background dielectric constant, $\gamma = 1/\tau_s = e/\mu m^*$ is the electron scattering rate, e is the electron charge, m^* is the electron effective mass, μ is the electron mobility. The plasma frequency is calculated as [31]:

$$\omega_p^2 = \frac{Ne^2}{\varepsilon_0 \varepsilon_\infty m^*} \quad (3)$$

which is obviously dependent on concentration of free carriers in the GaAs. Eventually, the conductivity is expressed by $\sigma(\omega) = \omega \varepsilon_0 \varepsilon_{imag}(\omega)$ [33].

Table 1. Simulation parameters of GaAs [14, 31, 34, 35]

Parameter	*Symbol*	*Value*
Background dielectric	ε_∞	12.9
Electron effective mass	m^*	0.067 m_0
Absorption coefficient	α [μm^{-1}]	1.3
Electron mobility	μ [$cm^2/V.s$]	8500
Carrier lifetime	τ [ps]	110
Reflectance	R	0.7

3 Results and Discussions

We first investigate the characteristics of the device without optical pumping. In this configuration, the structural parameters are designed in such a way that the resonant frequency occurs around 1 THz which is our frequency of interest for a carrier wave. For this purpose, the square lattice constant and radius of rods are selected as 96 µm and r=0.2a=19.2 µm respectively. It is assumed that Si is lossless and non-dispersive with a refractive index of n= 3.4 in the THz region [36]. The computing area includes 15 × 11 silicon rods, which are surrounded by scattering boundary conditions (SBC). We used the GaAs with a thickness of 3 µm and a width of 29 µm as a photoconductive substance. Because the radius of two outer rods r_c of the cavity can affect the device performance, we explored the transmittance spectra for three different values of radius r_c=13, 14, and 15 µm under the normal incidence of TE polarization using the 2-D finite element numerical method. According to figure 2(a), when the radius increases, the cavity demonstrates a stronger effect, resulting in narrower bandwidth and a redshift of the resonance frequency. The insertion loss is determined to be 2.2 dB at 1 THz for r_c=14 µm, based on the equation of IL =-10×log (I_{out}/I_{in}), where I_{out} and I_{in} are the transmitted THz power and the input THz power. Figure 2(b) illustrates normalized electric field ($|E|/|E_{inc}|$) distribution at 1 THz for r_c=14 µm. Here, $|E|$ and $|E_{inc}|$ represent the local electric field and the incident electric field, respectively. It can be seen that within the cavity, the THz field enhancement reaches up to 16, which is beneficial to the photoconductive-based modulators. Note that to confine the THz wave in the vertical direction, the aspect ratio of the rods should be sufficiently large, which has a feasible fabrication process [37-39].

Changing the w and h, give the extra degrees of freedom to smoothly control the properties of the cavity. We evaluated the quality factor (Q) from the transmittance spectrum according to $Q=\omega_0/\Delta\omega$. Figure 3 shows the tunability of the resonance frequency and quality factor in terms of the GaAs width for three selected thicknesses of h=3, 3.2, and 3.5 µm. As illustrated in this figure, the wider GaAs provides higher Q values and shifts the resonant frequency toward lower ones. The greater the Q, the longer the trapping time of the THz wave (i.e., $Q=\omega_0\tau$), which increases the interaction with the photoconductor material. Thus, forgoing the higher modulation speed, the modulator can operate with lower external optical power. As also observed from this figure, with an increase in the thickness of the GaAs, the quality factor

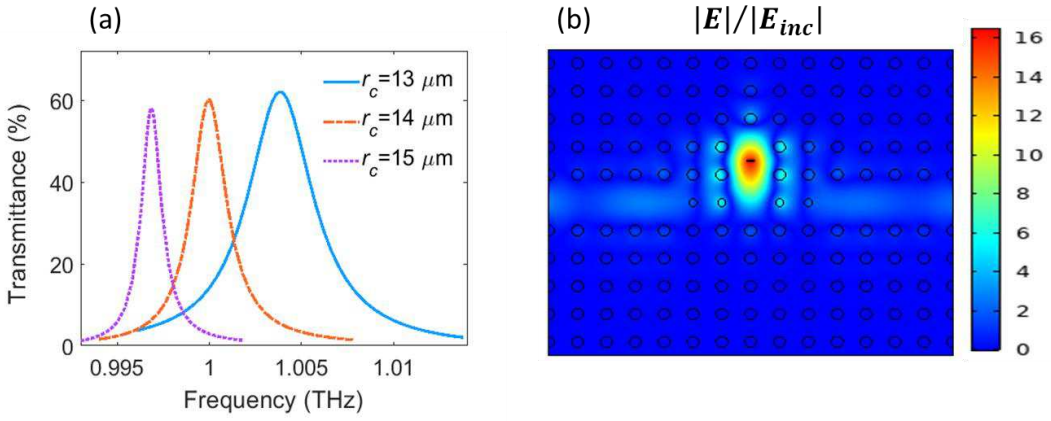

Fig. 2. (a) Transmittance spectra without optical pumping for r_c=13, 14, and 15 µm. (b) Normalized electric field distribution for r_c=14 µm at 1 THz.

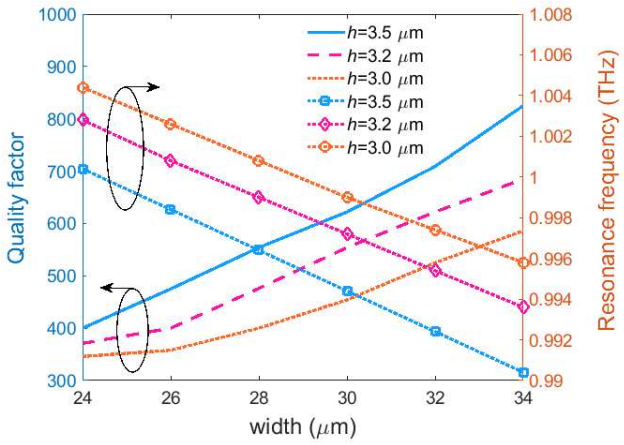

Fig. 3. Quality factor (left axis) and resonance frequency (right axis) versus the width of the GaAs for three thicknesses h=3, 3.2, and 3.5 μm without laser pumping.

increases, and the resonant frequency experiences a redshift. A comparison of plots for h= 3 and 3.5 μm at w=29 μm shows that the Q value enhances from 430 to about 590, while the resonance frequency drops from 1 THz to 0.995 THz.

Now, we can evaluate the performance of this modulator under the excitation of an optical pump. The most common way to excite massive free carriers is using a femtosecond laser as an optical pumping source. However, it is more practical to use a continuous wave (CW) laser instead of a femtosecond laser for modulation at GHz rate. We considered a CW laser at the center wavelength of 800 nm (higher photon energy with respect to GaAs bandgap: E_g=1.4 eV) for irradiating the GaAs. Based on the equations mentioned in the previous section, one can calculate the conductivity of the GaAs material for any given optical intensity. Figure 4(a) illustrates the carrier density and surface conductivity of the GaAs for a 1 THz wave as a function of pump intensity. As observed from this figure, the higher intensity generates more free carriers and the conductivity will increase. These results indicate that a low pump intensity in a given range generates a carrier density of about 10^{14} cm^{-3}, and then we will show that this low concentration leads to efficient intensity modulation of THz wave. Figure 4(b) illustrates the GaAs conductivity under applying a pump intensity of 40 W/cm^2 as a function of distance from the surface of GaAs and illumination time. It can be easily observed that the conductivity near the surface dramatically enhances when the illumination time is more than the carrier lifetime. Figure 4(c) shows the surface conductivity of GaAs overtime for three pump intensities of 60, 40, and 20 W/cm^2. As expected, the extra generated carriers over the illumination time enhance the conductivity, and finally, it reaches a steady state. The conductivity versus distance from the GaAs surface under different pump intensities has been plotted in figure 4(d). The conductivity increases with optical intensity, meanwhile decreasing with the distance from the surface. As observed from this figure, under the pump intensity of 40 W/cm^2, the surface conductivity at the steady-state is approximately 180 S/m. At distances of 1 and 2 μm from the surface, this value reaches 50 S/m and 20 S/m, respectively.

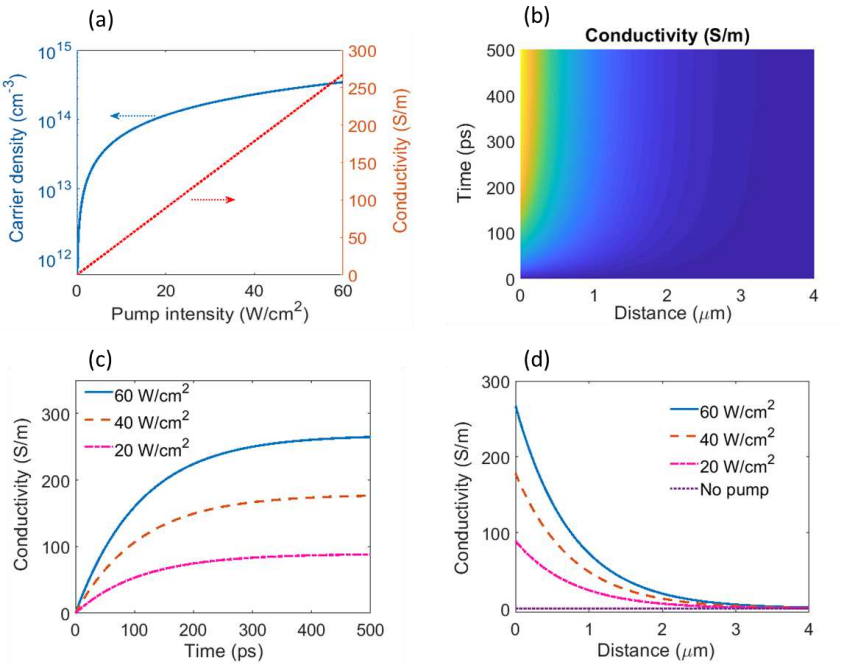

Fig. 4. (a) Carrier density (left axis) and surface conductivity (right axis) of the GaAs versus pump intensity. (b) Conductivity of the GaAs at 1 THz depending on the time and distance of the surface under application with a pump intensity of 40 W/cm^2. (c) Temporal dependence of surface conductivity at pump intensities of 60, 40, and 20 W/cm^2. (d) steady-state conductivity as a function of distance under various pump intensities.

Figure 5 shows the transmittance spectra in the steady-state under different pump intensities. Without pumping power, the THz wave is guided through the waveguide with a transmit peak of around 60% at 1 THz. By increasing the pumping power, the transmission of the THz wave will be gradually reduced, and finally, the transparency of this frequency window will be completely suppressed. Applying pumping power intensities of 10, 30, and 50 W/cm^2, the transmission peak drops to 36%, 17%, and 10% respectively. This behavior is due to the photoresponse of GaAs. Higher optical powers enhance the conductivity, resulting in greater absorptance and reflectance of the THz wave when transmitted through the waveguide. Due to the strong interaction of the THz wave with GaAs in the resonant cavity, the

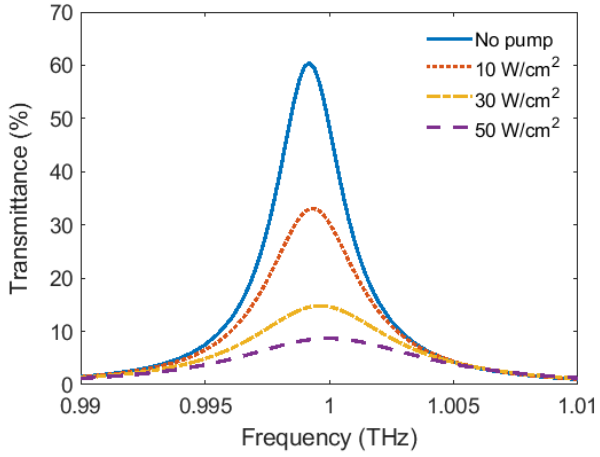

Fig. 5. Transmittance spectra without optical power intensity and under different intensities for r_c=14 µm.

transmitted THz wave suffers a significant reduction. Moreover, after illumination, there is almost no frequency shift of the transmittance spectra that would adversely affect the properties of the modulator. Because of the appropriate narrowband transmittance, the proposed modulator is especially suitable for THz CW signals.

In the absence of optical excitation, the GaAs are nearly transparent for the THz wave propagation, and there is no absorption loss as shown in figure 6(a). However, under the continuous wave laser pumping of 50 W/cm^2, THz power dissipation in GaAs reaches 36% at 1 THz. The absorptance of the GaAs is calculated as follow [40]:

$$\boldsymbol{A} = \frac{\iiint_{\boldsymbol{V_{abs}}} \frac{1}{2}\boldsymbol{\omega}|E|^2 imag(\varepsilon) dV}{\boldsymbol{P_{inc}}} \qquad (4)$$

with ω being the angular frequency, $imag(\varepsilon)$ is the imaginary part of the permittivity of the GaAs, $|E|$ the electric field amplitude, and the integral is applied over the absorption region V_{abs}. Figure 6(b) shows the changes in reflectance with the application of the same pumping. The reflectance has a low value of about 3% at 1 THz and rises to about 39% after applying a pump intensity of 50 W/cm^2.

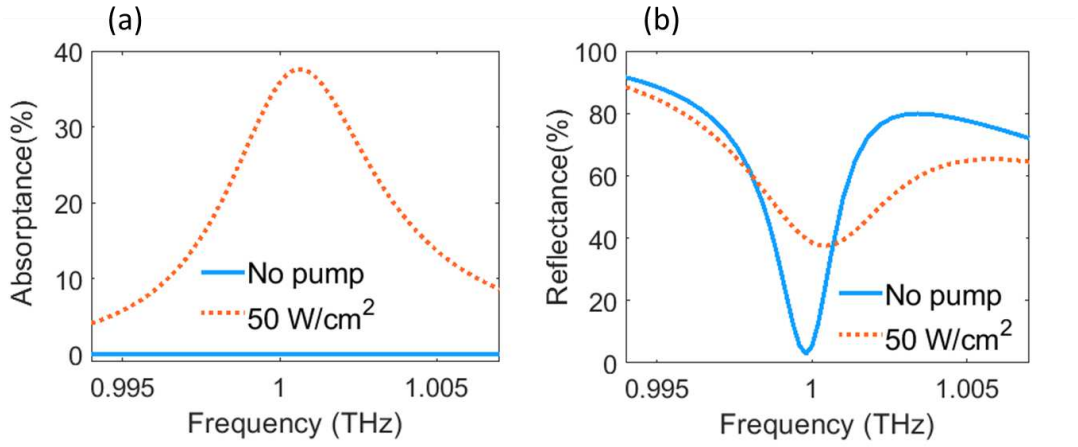

Fig. 6. (a) Absorptance power spectra, and (b) Reflectance power spectra when no pump and under applying a laser intensity of 50 W/cm^2 with r_c=14 µm.

Figure 7 illustrates the modulation depths under pumping up to 120 W/cm^2 for different values of r_c at their corresponding resonance frequency. Based on the modulator behavior, higher pump intensities reduce the transmitted THz power, which results in greater modulation depth. This figure also shows that under a relatively small intensity of 40 W/cm^2, the modulation depths enhance rapidly and reach the high values of around 89.5%, 79.1%, and 62.2% for r_c=15, 14, and 13 µm, respectively. Subsequently, by further increasing the optical intensity, the modulation depth tends to be saturated at higher values, which is high enough for all-optical THz modulators. As it can be observed from this figure, for a given intensity, a higher modulation depth can be achieved for the larger outer rods. This is due to the strong interaction of THz wave and photoconductive material for a greater r_c as mentioned before.

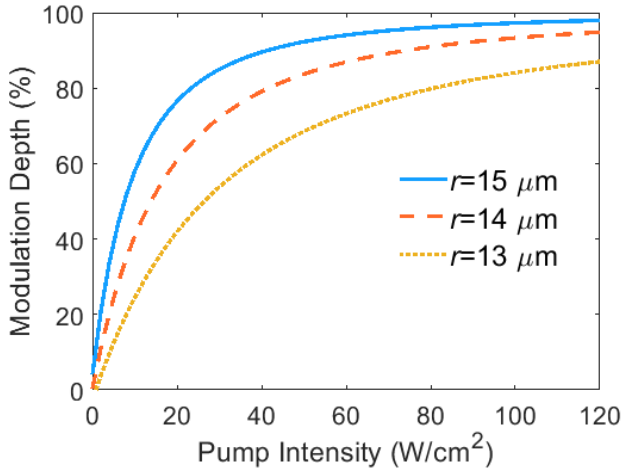

Fig. 7. Modulation depths with pumping intensity for r_c=13, 14, and 15 μm at their corresponding resonance frequency.

Modulation rate is another key parameter of the THz modulator that indicates the ability to follow a high-speed modulating signal. The modulation rate of the proposed device depends on the lifetime of free carriers and is also influenced strongly by the trapping time of the THz wave in the cavity. Since the carrier lifetime is greater than the cavity lifetime, the response time of the modulator is controlled by the free carrier lifetime. In this modulator, high-speed modulation in GHz frequency along with high modulation depth is possible even with low external power. We evaluate the dynamic response of the proposed modulator under the modulated square laser pulses with a duty cycle of 50% as shown in Figure 8(a). The rise and fall times of the THz intensity are attained by solving equation 1, which is related to

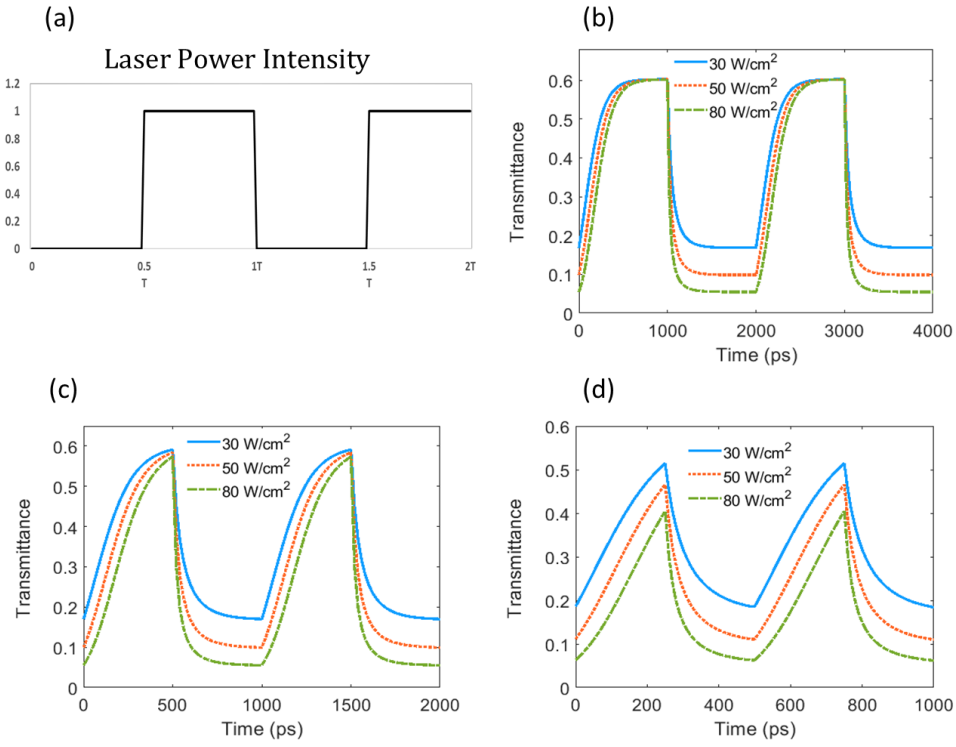

Fig. 2. (a) Laser power intensity with a duty cycle of 50%. Modulated intensity of 1 THz wave with different laser power intensities of (b) 0.5 GHz. (c) 1 GHz. (d) 2 GHz.

the excess carrier concentration and the carrier lifetime. When the illumination laser is off, the intensity of the transmitted THz wave increases and reaches a steady state. Afterward, during the illumination time of the laser, the carrier concentration increases as a function of time, and therefore the THz intensity drops to lower values which is dependent on the pump power intensity. The intensity of the transmitted THz wave under laser power of 30, 50, and 80 W/cm^2 at modulation frequencies of 0.5, 1, and 2 GHz are illustrated in Figure 8(b-d). One can notice that a lower modulation depth is achieved when the modulation speed increase from 0.5 GHz to 2 GHz. For the modulation rate of 0.5 GHz, the transmitted terahertz intensity is a square wave. As the modulation rate increases to 2 GHz, the modulated terahertz waveform becomes a semi-triangle wave.

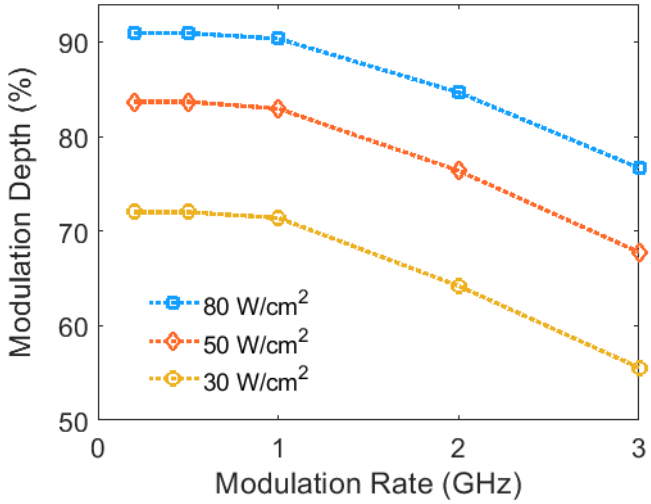

Fig .3. Pump power-dependent characteristics of the modulator at 1 THz.

Based on the above-mentioned analysis, this modulator demonstrates a pump power-dependent modulation effect. Figure 9 shows the device performance characteristics at 1 THz under various modulation rates up to 3 GHz. This figure indicates that by increasing the modulation rate up to 1 GHz, the modulator exhibits no drop in modulation depth, but at higher rates, modulation depth decreases strongly. This is because the illumination time becomes lower at a higher modulation rate, and thus fewer free carriers are generated. Figure 9 also shows that the change in pumping power has a considerable modulatory effect. Higher modulation depths appear as pumping reaches a higher level. Therefore, according to the modulation depth requirement, a laser with the proper optical power should be chosen. As a comparison, for a modulation rate of 0.5 GHz, varying the laser power intensity from 30 W/cm^2 to 80 W/cm^2, modulation depths in the range of 72% to 91% could be obtained, while at the rate of 3 GHz and under the same laser power, modulation depths of 56% to 77% will be achieved.

4 Conclusion

In summary, we designed and investigated a high-speed and highly efficient THz intensity modulator with external power-dependent characteristics. The proposed structure is composed of a photonic crystal cavity that makes a strong interaction between THz waves and included photoconductor GaAs. It has been demonstrated that increasing the conductivity of GaAs by laser illumination, causes the strong modulation

of THz waves. We can engineer the structural parameters for the desired function. Furthermore, numerical investigation at 1 THz exhibited excellent performance, with the ability to follow a high-speed modulating signal up to 3 GHz. Numerical results showed that under the optical power intensity of 80 W/cm^2, the modulator could achieve a high modulation depth of more than 90% with a speed of 1 GHz. When the modulation speed increases to 3 GHz, a modulation depth of about 76% can also be acquired. Also, higher modulation depths of up to 99% are achievable with this modulator by increasing the optical power. These unique characteristics of the modulator make it a good choice for developing future high-speed and energy-efficient THz communication systems.

Declarations

Authors Contributions Faramarz Alihosseini and Zahra Heshmatpanah developed the theoretical formalism and performed the numerical simulations. Hesam Zandi contributed to the final version of the manuscript.

Data Availability The datasets generated during the current study are available from the corresponding author on reasonable request.

Conflict of Interest The authors declare no competing interests.

Ethics Approval Not applicable

Consent to Participate Not applicable

Consent for Publication Not applicable

References

1. S. Koenig, D. Lopez-Diaz, J. Antes, F. Boes, R. Henneberger, A. Leuther, A. Tessmann, R. Schmogrow, D. Hillerkuss, R. Palmer, T. Zwick, C. Koos, W. Freude, O. Ambacher, J. Leuthold, and I. Kallfass, "Wireless sub-THz communication system with high data rate," Nature Photonics **7**, 977-981 (2013).
2. I. F. Akyildiz, J. M. Jornet, and C. Han, "Terahertz band: Next frontier for wireless communications," Physical Communication **12**, 16-32 (2014).
3. Z. T. Ma, Z. X. Geng, Z. Y. Fan, J. Liu, and H. D. Chen, "Modulators for Terahertz Communication: The Current State of the Art," Research **2019**, 6482975 (2019).
4. G. Isić, G. Sinatkas, D. C. Zografopoulos, B. Vasić, A. Ferraro, R. Beccherelli, E. E. Kriezis, and M. Belić, "Electrically Tunable Metal–Semiconductor–Metal Terahertz Metasurface Modulators," IEEE Journal of Selected Topics in Quantum Electronics **25**, 1-8 (2019).
5. J. Ji, S. Zhou, W. Wang, C. Luo, Y. Liu, F. Ling, and J. Yao, "Active multifunctional terahertz modulator based on plasmonic metasurface," Opt. Express **27**, 2363-2373 (2019).
6. N. Born, M. Scheller, M. Koch, and J. V. Moloney, "Cavity enhanced terahertz modulation," Applied Physics Letters **104**, 103508 (2014).
7. B. Sensale-Rodriguez, R. Yan, M. M. Kelly, T. Fang, K. Tahy, W. S. Hwang, D. Jena, L. Liu, and H. G. Xing, "Broadband graphene terahertz modulators enabled by intraband transitions," Nat Commun **3**, 780 (2012).

8. D.-S. Yang, T. Jiang, and X.-A. Cheng, "Optically controlled terahertz modulator by liquid-exfoliated multilayer WS2 nanosheets," Opt. Express **25**, 16364-16377 (2017).

9. J. Yue, F. Ling, and J. Yao, "All-optical tunable terahertz modulator based on a BiFeO3/Si heterostructure," Opt. Mater. Express **10**, 2919-2927 (2020).

10. S. Savo, D. Shrekenhamer, and W. J. Padilla, "Liquid Crystal Metamaterial Absorber Spatial Light Modulator for THz Applications," Advanced Optical Materials **2**, 275-279 (2014).

11. J. Yang, P. Wang, S. Gao, G. Deng, H. Lu, W. Lai, Z. Yin, Y. Li, and Y. Hu, "Tunable Terahertz Transmission Properties of Double-Layered Metal Hole-Loop Arrays Using Nematic Liquid Crystal," Journal of Infrared, Millimeter, and Terahertz Waves **40**, 276-287 (2019).

12. L. Xiong, B. Zhang, H. Ji, W. Wang, X. Liu, S. He, and J. Shen, "Active Optically Controlled Broadband Terahertz Modulator Based on Fe3O4 Nanoparticles," IEEE Transactions on Terahertz Science and Technology **8**, 535-540 (2018).

13. P. K. Singh, and S. Sonkusale, "High Speed Terahertz Modulator on the Chip Based on Tunable Terahertz Slot Waveguide," Scientific Reports **7**, 40933 (2017).

14. L. Fekete, F. Kadlec, P. Kužel, and H. Němec, "Ultrafast opto-terahertz photonic crystal modulator," Opt. Lett. **32**, 680-682 (2007).

15. H.-m. Chen, J. Su, J.-l. Wang, and X.-y. Zhao, "Optically-controlled high-speed terahertz wave modulator based on nonlinear photonic crystals," Opt. Express **19**, 3599-3603 (2011).

16. T. Chen, P. Liu, J. Liu, and Z. Hong, "A terahertz photonic crystal cavity with high Q-factors," Applied Physics B **115**, 105-109 (2014).

17. L. Deng, J. Teng, H. Liu, Q. Y. Wu, J. Tang, X. Zhang, S. A. Maier, K. P. Lim, C. Y. Ngo, S. F. Yoon, and S. J. Chua, "Direct Optical Tuning of the Terahertz Plasmonic Response of InSb Subwavelength Gratings," Advanced Optical Materials **1**, 128-132 (2013).

18. Y. Zhang, S. Qiao, S. Liang, Z. Wu, Z. Yang, Z. Feng, H. Sun, Y. Zhou, L. Sun, Z. Chen, X. Zou, B. Zhang, J. Hu, S. Li, Q. Chen, L. Li, G. Xu, Y. Zhao, and S. Liu, "Gbps Terahertz External Modulator Based on a Composite Metamaterial with a Double-Channel Heterostructure," Nano Letters **15**, 3501-3506 (2015).

19. Q.-Y. Wen, W. Tian, Q. Mao, Z. Chen, W.-W. Liu, Q.-H. Yang, M. Sanderson, and H.-W. Zhang, "Graphene based All-Optical Spatial Terahertz Modulator," Scientific Reports **4**, 7409 (2014).

20. J. Qiao, S. Wang, Z. Wang, C. He, S. Zhao, X. Xiong, S. Wang, X. Zhang, and X. Tao, "Ultrasensitive and Broadband All-Optically Controlled THz Modulator Based on MoTe2/Si van der Waals Heterostructure," Advanced Optical Materials **8**, 2000160 (2020).

21. D. S. Jessop, S. J. Kindness, L. Xiao, P. Braeuninger-Weimer, H. Lin, Y. Ren, C. X. Ren, S. Hofmann, J. A. Zeitler, H. E. Beere, D. A. Ritchie, and R. Degl'Innocenti, "Graphene based plasmonic terahertz amplitude modulator operating above 100 MHz," Applied Physics Letters **108**, 171101 (2016).

22. Y. Cao, S. Gan, Z. Geng, J. Liu, Y. Yang, Q. Bao, and H. Chen, "Optically tuned terahertz modulator based on annealed multilayer MoS2," Scientific Reports **6**, 22899 (2016).

23. E. Herrmann, H. Gao, Z. Huang, S. R. Sitaram, K. Ma, and X. Wang, "Modulators for mid-infrared and terahertz light," Journal of Applied Physics **128**, 140903 (2020).

24. Q. Guo, Z. Qin, Z. Wang, Y.-X. Weng, X. Liu, G. Xie, and J. Qiu, "Broadly Tunable Plasmons in Doped Oxide Nanoparticles for Ultrafast and Broadband Mid-Infrared All-Optical Switching," ACS Nano **12**, 12770-12777 (2018).

25. M. Ono, M. Hata, M. Tsunekawa, K. Nozaki, H. Sumikura, H. Chiba, and M. Notomi, "Ultrafast and energy-efficient all-optical switching with graphene-loaded deep-subwavelength plasmonic waveguides," Nature Photonics **14**, 37-43 (2020).

26. S. Li, H. Liu, Q. Sun, and N. Huang, "A Tunable Terahertz Photonic Crystal Narrow-Band Filter," IEEE Photonics Technology Letters **27**, 752-754 (2015).

27. H. Li, M. X. Low, R. T. Ako, M. Bhaskaran, S. Sriram, W. Withayachumnankul, B. T. Kuhlmey, and S. Atakaramians, "Broadband Single-Mode Hybrid Photonic Crystal Waveguides for Terahertz Integration on a Chip," Advanced Materials Technologies **5**, 2000117 (2020).

28. Y. Wang, D. Zhang, B. Xu, Z. Dong, J. Pei, and S. Xu, "T-typed photonic crystal circulator with square lattice Al2O3 rods array and NiZn-ferrite posts," Materials & Design **181**, 107978 (2019).

29. B. You, D. Liu, T. Hattori, T.-A. Liu, and J.-Y. Lu, "Investigation of spectral properties and lateral confinement of THz waves on a metal-rod-array-based photonic crystal waveguide," Opt. Express **26**, 15570-15584 (2018).

30. S.-H. Yang, and M. Jarrahi, "Spectral characteristics of terahertz radiation from plasmonic photomixers," Opt. Express **23**, 28522-28530 (2015).

31. Y. C. Jun, E. Gonzales, J. L. Reno, E. A. Shaner, A. Gabbay, and I. Brener, "Active tuning of mid-infrared metamaterials by electrical control of carrier densities," Opt. Express **20**, 1903-1911 (2012).

32. E. Lee, I. C. Seo, S. C. Lim, H. Y. Jeong, and Y. C. Jun, "Active switching and tuning of sharp Fano resonances in the mid-infrared spectral region," Opt. Express **24**, 25684-25696 (2016).

33. J.-s. Li, and M.-s. Hu, "Enhancement of silicon modulating properties in the THz range by YAG-Ce coating," Scientific Reports **10**, 6605 (2020).

34. C.-H. Liu, Y.-C. Chang, S. Lee, Y. Zhang, Y. Zhang, T. B. Norris, and Z. Zhong, "Ultrafast Lateral Photo-Dember Effect in Graphene Induced by Nonequilibrium Hot Carrier Dynamics," Nano Letters **15**, 4234-4239 (2015).

35. Q. Meng, Y. Zhang, Z. Zhong, and B. Zhang, "Optically tuneable broadband terahertz metamaterials using photosensitive semiconductor material," Journal of Modern Optics **65**, 2086-2092 (2018).

36. A. C. Tasolamprou, A. D. Koulouklidis, C. Daskalaki, C. P. Mavidis, G. Kenanakis, G. Deligeorgis, Z. Viskadourakis, P. Kuzhir, S. Tzortzakis, M. Kafesaki, E. N. Economou, and C. M. Soukoulis, "Experimental Demonstration of Ultrafast THz Modulation in a Graphene-Based Thin Film Absorber through Negative Photoinduced Conductivity," ACS Photonics **6**, 720-727 (2019).

37. C. Kraeh, M. Schieber, A. Popescu, H. Hedler, and J. Finley, "Photonic crystal materials realized by high aspect ratio micro-rod arrays," in *IEEE Photonics Conference 2012*(2012), pp. 723-724.

38. K. Cui, Y. Li, X. Feng, Y. Huang, and W. Zhang, "Fabrication of high-aspect-ratio double-slot photonic crystal waveguide in InP heterostructure by inductively coupled plasma etching using ultra-low pressure," AIP Advances **3**, 022122 (2013).

39. G. Si, A. J. Danner, S. L. Teo, E. J. Teo, J. Teng, and A. A. Bettiol, "Photonic crystal structures with ultrahigh aspect ratio in lithium niobate fabricated by focused ion beam milling," Journal of Vacuum Science & Technology B **29**, 021205 (2011).

40. J. Guo, Z. Wu, and Y. Zhao, "Enhanced light absorption in waveguide Schottky photodetector integrated with ultrathin metal/silicide stripe," Opt. Express **25**, 10057-10069 (2017).